

## TOPOLOGICAL INFERENCE FOR EEG AND MEG<sup>1</sup>

BY JAMES M. KILNER AND KARL J. FRISTON

*University College London*

Neuroimaging produces data that are continuous in one or more dimensions. This calls for an inference framework that can handle data that approximate functions of space, for example, anatomical images, time–frequency maps and distributed source reconstructions of electromagnetic recordings over time. Statistical parametric mapping (SPM) is the standard framework for whole-brain inference in neuroimaging: SPM uses random field theory to furnish  $p$ -values that are adjusted to control family-wise error or false discovery rates, when making topological inferences over large volumes of space. Random field theory regards data as realizations of a continuous process in one or more dimensions. This contrasts with classical approaches like the Bonferroni correction, which consider images as collections of discrete samples with no continuity properties (i.e., the probabilistic behavior at one point in the image does not depend on other points). Here, we illustrate how random field theory can be applied to data that vary as a function of time, space or frequency. We emphasize how topological inference of this sort is invariant to the geometry of the manifolds on which data are sampled. This is particularly useful in electromagnetic studies that often deal with very smooth data on scalp or cortical meshes. This application illustrates the versatility and simplicity of random field theory and the seminal contributions of Keith Worsley (1951–2009), a key architect of topological inference.

**1. Introduction.** This paper is about inferring treatment effects or responses that are expressed in image data. The problem we consider is how to accommodate the multiplicity of data and correlations due to smoothness, when adjusting for the implicit multiple comparison problem. The data we have in mind here are images that can be treated as discrete samples from a function of some underlying support: for example, two-dimensional images of the brain sampled from evenly spaced points (i.e., a grid) in anatomical

---

Received August 2009; revised January 2010.

<sup>1</sup>Supported by The Wellcome Trust.

*Key words and phrases.* Random field theory, topological inference, statistical parametric mapping.

|   |
|---|
| <p>This is an electronic reprint of the original article published by the <a href="#">Institute of Mathematical Statistics</a> in <i>The Annals of Applied Statistics</i>, 2010, Vol. 4, No. 3, 1272–1290. This reprint differs from the original in pagination and typographic detail.</p> |
|---|

space. In brief, the multiple comparison problem can be dissolved by modeling the data as samples from random fields with known (or estimable) covariance functions over their support. This allows one to use results from random field theory to determine the topological behavior (e.g., the number of peaks above some threshold) of summary statistic images, under the null hypothesis. Because we treat the data and derived statistical processes as implicit functions of some metric space, this approach is closely related to functional data analysis [Ramsay and Silverman (2005)]. When this functional perspective is combined with random field theory (as a probabilistic model of data), we get a generic inference framework (topological inference) that is used widely in brain mapping and other imaging fields.

We will review topological inference in neuroimaging with a special focus on electromagnetic (EEG and MEG) data. In particular, we stress the generality of this approach and show that random theory can be applied to data-features commonly used in EEG and MEG. These data include interpolated scalp-maps, time–frequency maps of single-channel data, cortically constrained maps of current density, source reconstruction on the cortex or brain volume, etc. Irrespective of the underlying geometry or support of these data, the topological behavior of their associated statistical parametric maps is invariant. This means one can apply established procedures directly to make inferences about evoked and induced responses in sensor or source-space. This reflects the simplicity and generality of topological inference and provides a nice vehicle to illustrate the seminal work of Keith Worsley, who sadly passed away shortly before this article was written.

Conventional whole-brain neuroimaging data analysis uses some form of statistical parametric mapping. This entails a parametric model (usually a general linear model) of data at each point in image space to produce a statistical parametric map (usually of a Student’s  $t$ -statistic). Topological inference about regional effects then uses random field theory to control for the implicit multiple comparisons problem. This is standard practice in imaging modalities like functional magnetic resonance imaging (fMRI) and positron emission tomography. However, the application to electroencephalography (EEG) and magnetoencephalography (MEG) data is relatively new. An interesting feature of electromagnetic data is that they are often formulated on meshes or manifolds, which may seem to complicate the application of random field theory. This paper shows that random field theory can be applied directly to electromagnetic data on manifolds and that it accommodates the anisotropic and complicated spatial dependencies associated with smooth electromagnetic data-features. We have chosen to illustrate topological inference on electromagnetic data-features because they are inherently smooth and show profound spatial dependencies, which preclude classical procedures. These dependencies arise from preprocessing steps (e.g., interpolation to produce scalp maps or source reconstruction, under regularizing

smoothness constraints) or from the nature of the data-features per se (e.g., physiological smoothness in time-series or time–frequency smoothness induced by wavelet decomposition).

EEG and MEG are related noninvasive neuroimaging techniques that provide measures of human cortical activity. EEG and MEG typically produce a time-varying modulation of signal amplitude or frequency-specific power in some peristimulus period, at each electrode or sensor. The majority of researchers are interested in whether condition-specific effects (observed at particular sensors and peristimulus times) are statistically significant. However, this inference must correct for the number of statistical tests performed. In other words, the family-wise error (FWE) rate should be controlled. For independent observations, the FWE rate scales with number of observations. A simple but inexact method for controlling FWE is a Bonferroni correction. However, this procedure is rarely adopted in neuroimaging because it assumes that neighboring observations are independent: when there is a high degree of correlation among neighboring samples (e.g., when data-features are smooth), the correction is far too conservative.

Although the multiple comparisons problem has always existed for EEG/MEG analyses (due to the number of time bins in the peristimulus time window), the problem has become more acute with the advent of high-density EEG-caps and MEG sensor arrays that increase the number of observations across the scalp. In many analyses, the multiple comparisons problem is circumvented by restricting the search-space prior to inference, so that there is only one test per repeated measure. This is usually accomplished by averaging the data over pre-specified sensors and time-bins of interest. This produces one summary statistic per subject per condition. In many instances, this is a powerful and valid way to side-step the multiple comparisons problem; however, it requires the space-of-interest be specified a priori. A principled specification of this space could use orthogonal or independent data-features. For example, if one was interested in the attentional modulation of the N170 (a typical event-related wave recorded 170 ms after face presentation), one could first define the electrodes and time-bins that expressed a N170 (compared to baseline) and then test for the effects of attention on their average. Note that this approach assumes that condition-specific effects occur at the same sensors and time and is only valid when selection is not biased [see Howell (1997); Kriegeskorte et al. (2009)]. In situations where the location of evoked or induced responses is not known a priori, or cannot be localized independently, one can use topological inference to search over some space for significant responses; this is the approach we consider.

This paper comprises two sections. The first reviews the application of random-field theory [RFT; Worsley et al. (1992, 1996)] to statistical parametric maps [SPMs; Friston et al. (1991, 1994)] of MEG/EEG data over

space, time and frequency. In the second section we illustrate the basic procedures by applying RFT to SPMs of MEG/EEG data and try to highlight the generality of the approach. In this article we focus on FWE but note the same topological thinking and random field theory results can also be used to control false discovery rate [FDR; Benjamini and Hochberg (1995)]. We provide a brief review of Topological FDR for image analysis in the discussion.

**2. Random fields and topological inference.** In this section we review RFT and its central role in statistical parametric mapping. We first provide a heuristic overview and then give details, with a special focus on issues that relate to EEG/MEG analyses. RFT provides an established method for assigning  $p$ -values to topological features of SPMs in the analysis of functional magnetic resonance (fMRI) and other anatomical, metabolic or hemodynamic images. More recently, it has been applied to hierarchical models of EEG/MEG data [Park et al. (2002); Barnes and Hillebrand (2003); Kiebel and Friston (2004); Henson et al. (2007); Garrido et al. (2008)], global field power statistics [Carbonell et al. (2004)], time–frequency data [Kilner, Kiebel and Friston (2005)], current source density maps [Pantazis et al. (2005)] and even frequency by frequency coupling maps from dynamic causal modeling [Chen, Kiebel and Friston (2008)].

2.1. *Statistical parametric mapping.* Statistical parametric maps (e.g.,  $t$ -maps) are fields with values that are, under the null hypothesis, distributed according to a known probability distribution. This is usually the Student’s  $t$ - or  $F$ -distributions. SPMs are interpreted as continuous statistical processes by referring to the probabilistic behavior of random fields [Worsley et al. (1992, 1996); Friston et al. (1991, 1995)]. Usually, a general linear model is used to estimate the parameters that best explain some data-features. One fits a general linear model at each point (vertex or voxel) of the search-space and computes the usual statistics [see Friston et al. (1995) for details]; these constitute the SPM. The search-space can, in principle, be of any dimensionality and could be embedded in a higher dimensional space. RFT is then used to resolve the multiple comparisons problem that occurs when making inferences over the search-space: Adjusted  $p$ -values are obtained by using results for the expected Euler characteristic of the excursion set of a smooth statistical process.

The Euler characteristic (or Euler–Poincaré characteristic) is a topological invariant that describes the shape or structure of a manifold, regardless of the way it is stretched or distorted. It was defined classically for the surfaces of polyhedra, where it is simply the number of faces and corners, minus the number of edges. In our context, it effectively counts the number of connected regions (minus the number of holes) in the excursion set that remains

after thresholding an SPM. At very high thresholds the Euler characteristic (abbreviated here “EC”) basically reduces to the number of suprathreshold peaks and the expected EC becomes the probability of getting a peak above threshold by chance (under the Poisson clumping heuristic).

The expected EC therefore approximates the probability that the SPM exceeds some height by chance. This is the same as the  $p$ -value based on the null distribution of the maximum statistic over search-space. The ensuing  $p$ -values can be used to find a corrected height threshold or assign a corrected  $p$ -value to any observed peak in the SPM [see Worsley (2007) for an introduction to RFT]. The fundamental advantage of RFT is that it models continuous statistical processes and not a collection of individual statistics. This means that RFT can be used to characterize topological features of the SPM like peaks. The key intuition behind RFT procedures is that they control the false positive rate of topological features, not the tests themselves. By way of contrast, a Bonferroni correction controls the false positive rate of tests (at vertices, time–frequency bins or voxels), which would be unnecessarily conservative when the data are smooth. RFT has become a cornerstone of inference in human brain mapping that enables researchers to adjust their  $p$ -values to control false positive rates over many different sorts of search-spaces with spatial dependencies.

*2.2. Random field theory.* The assumptions under which the random field correction operates are quite simple and are satisfied by high-density EEG/MEG data because of their inherent smoothness in space and time. As noted above, the key null distribution is that of the maximum statistic over the search volume. By evaluating any observed statistic, in relation to the null distribution of its maximum, one is implicitly implementing a multiple comparisons procedure for continuous data. An analytic form of this distribution is derived using results from RFT. These results use the expected Euler characteristic of excursion sets above some specified threshold. For high thresholds this expectation is the same as the probability of getting a maximum statistic above threshold. By treating the data, under the null hypothesis, as continuous random fields, the distribution of the Euler characteristic of any statistical process derived from these fields can be used as an approximation to the null distribution required for inference. When using a general linear model the random (component) fields correspond to error fields. RFT assumes that these are a good lattice approximation of an underlying random field. Furthermore, the expressions require that the error fields are multivariate Gaussian with a differentiable autocorrelation function. It is a common misconception that this correlation function has to be Gaussian: it does not. Furthermore, the autocorrelation function does not have to be stationary or isotropic. The ensuing  $p$ -value is a function of the search volume, over any arbitrary number of dimensions, and the local smoothness

of the underlying error fields, which can be expressed in terms of full-width, half-maximum (FWHM). A useful concept that combines these two aspects of the search-space is the number of “resolution elements” (*resels*—see below). The resel count corresponds to the number of FWHM elements that comprise the search volume. Heuristically, these encode the number of independent observations. In other words, even a large search volume may contain a relatively small number of resels, if it is smooth. This calls for a much less severe adjustment to the  $p$ -value than would be obtained with a Bonferroni correction based on the number of bins, voxels or vertices.

We now develop these intuitions more formally, with a didactic summary of random field theory based on Taylor and Worsley (2007) and implemented in conventional software such as *fMRIStat*, *SurfStat* and *SPM8*. The associated software is available from <http://www.math.mcgill.ca/keith/fmristat/>, <http://www.math.mcgill.ca/keith/surfstat/> and <http://www.fil.ion.ucl.ac.uk/spm/>.

2.3. *The Euler characteristic.* Imagine that we have collected some EEG/MEG data and have interpolated them to produce a 2D scalp-map of responses at one point in peristimulus time for two conditions and several subjects. We now compare the two conditions with a statistical test; such that we now have  $T$  (test)-values at every vertex in our scalp-map. We are interested in the  $T$ -value, above which we can declare that differences are significant at some  $p$ -value that is adjusted for FWE.

RFT gives adjusted  $p$ -values by using results for the expected Euler characteristic (EC) of the excursion set of a smooth statistical process. The expected EC of the excursion set is an accurate approximation to the  $p$ -value of the maximum of a smooth, nonisotropic random field or SPM of some statistic  $T(s)$  at Euclidean coordinates  $s \in S$ , above a high threshold  $t$  and is given by

$$(1) \quad P\left(\max_{s \in S} T(s) \geq t\right) = \sum_{d=0}^D \ell_d(S, \Lambda) \rho_d(t),$$

where  $\ell_d(S, \Lambda)$  are the *Lipschitz–Killing curvatures* (LKC), of the  $D$ -dimensional search-space  $S \subset \mathfrak{R}^D$ , and  $\rho_d(u)$  are the *EC densities*. These are two important quantities: put simply, the LKC measures the topologically invariant “volume” of the search-space. In other words, it is a measure of the manifold or support of the statistical process that does not change if we stretch or distort it. The EC density is the corresponding “concentration” of events (excursions or peaks) we are interested in. Effectively, the product of the two is the number of events one would expect by chance (the expected Euler characteristic). When this number is small, it serves as our nominal false positive rate or  $p$ -value.

Equation (1) shows that the  $p$ -value receives contributions from all dimensions of the search-space, where the largest contribution is generally from the highest dimension ( $D$ ). In the example above, we had a two-dimensional  $D = 2$  search-space. Each contribution comprises two terms: (i) The LKC, which measures the effective volume, after accounting for non-isotropic smoothness in the component or error fields. This term depends on the geometry of the search-space and the smoothness of the errors but not the statistic or threshold used for inference. (ii) Conversely, the EC density, which is the expected number of threshold excursions per LKC measure, depends on the statistic and threshold but not the geometry or smoothness. Closed-form expressions for the EC density are available for all statistics in common use [see Worsley et al. (2002)].

2.4. *Smoothness and resels.* The LKC encodes information about the support and local correlation function of the underlying error fields  $Z(s)$ . The correlation structure is specified by their roughness or the variability of their gradients,  $\dot{Z}(s)$ , at each coordinate

$$(2) \quad \Lambda(s) = \text{Var}(\dot{Z}(s)).$$

In the isotropic case, when the correlations are uniform,  $\Lambda(s) = I_{D \times D}$ , the LKC reduces to *intrinsic volume*

$$(3) \quad \ell_d(S, I_{D \times D}) = \mu_d(S).$$

The intrinsic volume is closely related to the intuitive notion of a volume and can be evaluated for any regular manifold (or computed numerically given a set of vertices and edges defining the search-space). Note that when  $S$  is a  $D$ -dimensional manifold embedded in a higher dimensional space, the higher dimensional volumes are all zero, so that the sum in equation (1) need only go to the dimensionality of the manifold, rather than the dimensionality of the embedding space. In the example above, we can think of our 2D scalp map embedded in a 3D head-space; however, we only need consider the two dimensions of the scalp-map or manifold. The LKC term that makes the largest contribution to the  $p$ -value is the final volume term

$$(4) \quad \ell_D(S, \Lambda) = \int_S |\Lambda(s)|^{1/2} ds = (4 \ln 2)^{D/2} \text{resels}_D(S).$$

This generalization of the LKC is the resel count [Worsley et al. (1996)], which reflects the number of effectively independent observations. It can be seen from equation (4) that the resels (or LKC) increase with both volume and roughness.

2.5. *Estimating the resel count.* The resel count can be estimated by replacing the coordinates  $s \in S$  by normalized error fields  $u(s) \in \mathbb{R}^n$ , to create a new space

$$(5) \quad u(s) = \frac{Z(s)}{\sqrt{n}} \approx \frac{r(s)}{\|r(s)\|}.$$

Here,  $r(s)$  are  $n$  normalized residual fields from our general linear model. Crucially, the intrinsic volume at any point in this new space is the LKC

$$(6) \quad \ell_d(S, \Lambda) = \mu_d(u(s)).$$

This elegant device was proposed by Worsley et al. (1999). It says that to estimate the LKC, one simply replaces the Euclidean coordinates by the normalized residuals, and proceeds as if  $u(s)$  were isotropic. The basic idea is that  $u(s)$  can be thought of as an estimator of  $S$  in isotropic space, in the sense that the local geometry of  $u(s)$  is the same as the local geometry of  $S$ , relative to  $Z(s)$  [Taylor and Worsley (2007)]. This equivalence leads to the following estimator:

$$(7) \quad \ell_D(S, \Lambda) = \frac{1}{D!} \sum_{i=1}^N |\Delta u_i^T \Delta u_i|^{1/2},$$

where  $\Delta u = [\Delta u_1, \dots, \Delta u_D]$  are the finite differences between neighboring vertices of the  $N$  components that tile the search manifold (e.g., edges, triangles, tetrahedra, etc.), note that this approximation does not depend on the Euclidean coordinates of the vertices, only how they are connected to form components [Worsley et al. (1999)]. At present, the *SPM8* software (but not *SurfStat*) uses the following LKC estimator,

$$(8) \quad \ell_d(S, \Lambda) = \mu_d(S) \left( \frac{\ell_D(S, \Lambda)}{\mu_D(S)} \right)^{d/D},$$

and the approximation,  $\Delta u_i^T \Delta u_i \approx \Delta r_i^T \Delta r_i / r_i^T r_i$ , which assumes  $\|r_i\| \approx \|r_j\|$  for connected vertices; this is generally true, provided the error variance changes sufficiently smoothly.

The important result above is equation (6), which allows one to estimate the intrinsic volume of  $u(s)$ , which is the LKC of  $S$ . However, this is another perspective on equation (7) that comes from an estimator based on equation (4) [see Kiebel et al. (1999)],

$$(9) \quad \ell_D(S, \Lambda) = \sum_{i=1}^N |\Lambda(s_i)|^{1/2} \Delta S_i.$$

Comparison with equation (7) suggests that the determinant of finite differences can also be regarded as an estimate of the local roughness times the volume  $\Delta S_i$  of the  $i$ th component of search-space,

$$(10) \quad |\Lambda(s_i)|^{1/2} \Delta S_i = \frac{1}{D!} |\Delta u_i^T \Delta u_i|^{1/2}.$$

Effectively, the dependency of the local LKC on volume and the distances between vertices (implicit in evaluating the gradients) cancel, so that we need only consider the finite differences. *In short, the geometry encoded in the geodesic distances among vertices (or voxels) has no effect on the LKC or ensuing  $p$ -values.* This means we can take any nonisotropic statistical field defined on any  $D$ -dimensional manifold embedded in a high-dimensional space (e.g., a cortical mesh in anatomical space) and treat it as an isotropic  $D$ -dimensional SPM, provided we replace the gradients of the normalized residuals (which depend on the geometry) with finite differences among connected vertices (which do not). This invariant aspect of the resel count (or the LKC) estimator speaks to the topological nature of inference under random field theory. This is summarized nicely in Taylor and Worsley (2007):

“Note first that the domain of the random fields could be warped or deformed by a one-to-one smooth transform without fundamentally changing the nature of the problem. For example, we could ‘inflate’ the average cortical surface to a sphere and carry out all our analysis on the sphere. Or we could use any convenient shape: the maximum of the Student’s  $t$ -statistic would be unchanged, and so would the Euler characteristic of the excursion set. Of course the correlation structure would change, but then so would the search region, in such a way that the effects of these on the LKC, and hence the expected Euler characteristic, cancel.”

The fact that the resels are themselves a topological measure is particularly important for EEG and MEG data. This means that the resel count does not depend on the Euclidean coordinates or geometry of the data support. In other words, one can take data from the vertices of a cortical mesh embedded in a 3D space and treat it as though it came from a flat surface. This ability to handle nonisotropic correlations on manifolds with an arbitrary geometry reflects the topographic nature of RFT and may find a particularly powerful application in EEG and MEG research. In the next section we demonstrate the nature of this application.

**3. Illustrative applications.** In this section we illustrate RFT, as implemented in *SPM8*, to adjust  $p$ -values from SPMs of space-time MEG data. Data were recorded from 14 subjects (9 males, age range 25–45 yrs). All subjects gave informed written consent prior to testing under local ethical committee approval. MEG was recorded using 275 third-order axial gradiometers with the Omega275 CTF MEG system (VSMmedtech, Vancouver,

Canada) at a sampling rate of 480 Hz. Details of the experimental design will be found in Kilner, Marchant and Frith (2006). Here, we describe the features of the task that are relevant for the analyses used in this paper; namely, event-related analyses of right-handed button presses in the time and frequency domains.

Subjects performed four sessions of a task consecutively. In each session, subjects performed forty button presses with their right index finger, giving a total of 160 trials. All MEG analyses were performed in *SPM8*: First, the data were epoched relative to the button press. The data were band-pass filtered between 0.1 and 45 Hz using a time window of  $-500$  to  $1000$  ms and down-sampled to 100 Hz. For event-related field (ERF) analyses, the data were averaged across trials for each sensor. For time-frequency (TF) analyses, induced oscillations were quantified using a (complex Morlet) wavelet decomposition of the MEG signal, over a 1–45 Hz frequency range. The wavelet decomposition was performed for each trial, sensor and subject. The ensuing time-frequency maps were averaged across trials. For the purposes of this paper, we were interested in demonstrating significant “rebound” effects in the 15–30 Hz range [Salmelin and Hari (1994)]. Therefore, the time-frequency maps were averaged across the 15–30 Hz frequency band to produce a time-varying modulation of the so-called *Beta* power at each sensor.

For both the ERF and TF analyses, the sensor-data at each time bin were interpolated to produce a 2D sensor-space map on a  $64 \times 64$  mesh aligned to the left–right and anterior–posterior axes [e.g., Figure 1(C)]. A 3D data-array was generated for each subject by stacking these scalp-maps over peristimulus time [Figure 1(D)]. This produces a 3D image, where the dimensions are space (left–right and anterior–posterior) and time. For each subject, a second reference 3D image was generated that was the mean amplitude of the signal at each sensor, replicated at each time point. These space-time maps were smoothed using a Gaussian kernel (FWHM  $6 \times 6$  spatial bins and 60 ms) prior to analysis. This smoothing step is essential. First, it assures the assumptions of RFT are not violated. These assumptions are that the error fields conform to a good lattice approximation of a random field with a multivariate Gaussian distribution. Second, it blurs effects that are focal in space or time, ensuring overlap among subjects. It should be noted that although smoothing is an important pre-processing procedure, it is not an inherent part of topological inference: RFT estimates the smoothness directly from the (normalized residual) data, during the estimation of the resel count. This means one has the latitude to smooth in a way that emphasizes the data-features of interest. For example, with cortical or scalp manifolds one might use weighted [e.g., Pantazis et al. (2005)] or un-weighted graph-Laplacian operators to smooth the data on their meshes [see Harrison et al. (2008) for a fuller discussion]. An un-weighted graph-Laplacian

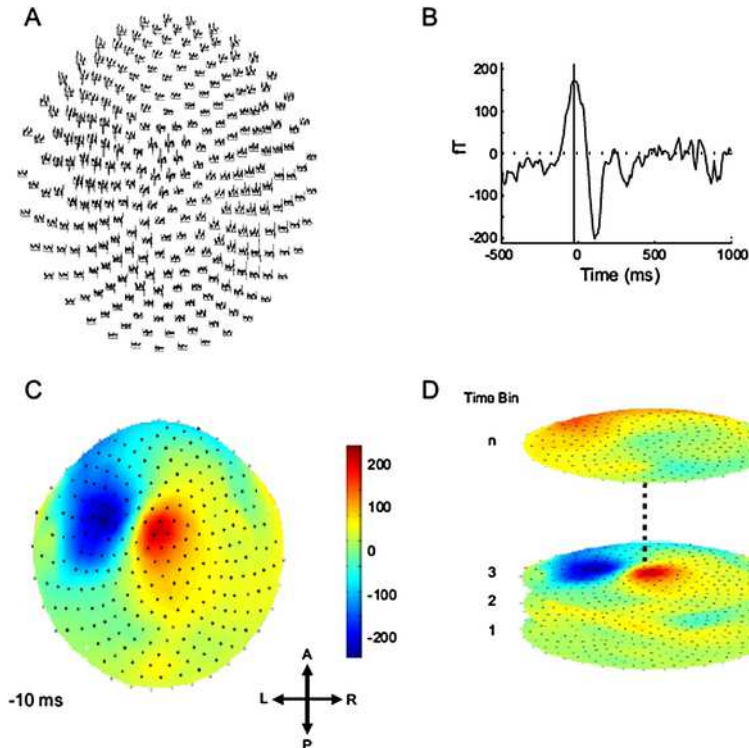


FIG. 1. *Single-subject ERF data.* (A) shows the average ERF for a single subject. The data are plotted for 275 sensors across peristimulus time. (B) shows the average ERF for the same subject from one sensor. The vertical line indicates the maximum positive value of this ERF. (C) shows the sensor-space interpolated map across all sensors at  $-10$  ms, indicated by the line in (B). (D) shows how the 3D sensor-space-time data volume is formed.

produces the same smoothing as convolution with a Gaussian kernel on a regular grid: this is the approach used here.

We then generated SPMs on a regular 3D grid by performing a series of  $t$ -tests comparing the response to the mean image at every bin in scalp-space and time. This is called a mass-univariate approach and is identical to that adopted in the analysis of fMRI data.

**3.1. Event-related field analysis.** The analysis of the ERF is typical of high-density EEG/MEG studies. Figure 1 illustrates the problem of making a statistical inference on such multidimensional data. The data for each subject consists of 151 observations across time at 275 observations in sensor-space [Figure 1(A)]. Figure 1(B) shows the time-course of the ERF at a sensor that evidences a movement-evoked field [e.g., Hari and Imada (1999)]. Note that the early onset is due to alignment to the button press and not

the onset of movement. If one looks at the modulation of this signal across space in the sensor-space map (at the maximum of the effect), a clear dipole field pattern can be seen [Figure 1(C)].

We now want to test for responses over space and time. An SPM for effects greater or less than the mean was calculated using a paired  $t$ -test over subjects. In this example, only one peak was greater than a threshold adjusted for the entire search volume [ $p < 0.05$  corrected; Figure 2(A)]. The peak value occurred 120 ms prior to the button press and was within a cluster of right frontal sensors [Figure 2(A) and Table 1]. Figure 2(B) shows the average (nonstandardized) effect size across sensor-space at  $-120$  ms: when comparing the thresholded SPM [Figure 2(A)] and the effect-size map [Figure 2(B)], it can be seen that the peaks of the SPM and effect-size are in different places. There is no reason why they should be in the same location, because the Student's  $t$ -statistic reflects the effect-size and standard error. This example highlights the benefit of inference that is controlled for FWE across space and time, namely, that one can discover effects that were not predicted a priori. However, it also suggests significant effects should be interpreted in conjunction with the effect-size. In other words, although the peak in the SPM tells us where differences are significant, it does not necessarily identify the maximum response in a quantitative sense.

In most instances, searches over SPMs are constrained or directed. This is common in fMRI when we know a priori where in the brain to look. The same is true for EEG/MEG data. For the example considered here, we may want to constrain the search-space to some peristimulus time window. However, in contradistinction to conventional approaches, we do not average over the volume of interest space but use it to constrain the search and increase its sensitivity. In this instance, the RFT adjusts  $p$ -values over a smaller volume and implements a less severe adjustment. For the ERF shown here, given the previous literature, we defined a time-window of interest of 200 ms, starting at  $-100$  ms before the button press. Within this time-window, the peak of the SPM occurred at 10 ms at central sensors overlying the left hemisphere and was significant at  $p < 0.05$  [corrected: Figure 2(C) and Table 2]. Figure 2(C) also shows the thresholded SPM at  $p < 0.001$  (uncorrected) for the opposite contrast, where responses were greater than the mean. When comparing this thresholded SPM image to the corresponding effect-size image [Figure 2(D)], one can see that the sensors that survive the threshold in Figure 2(C) display a classical single-dipole field pattern [Figure 2(D)].

*3.2. Time–frequency analysis.* Time–frequency analyses of EEG/MEG recordings induce a 4D search-space, at least two spatial dimensions, time and frequency [Figure 3(A)]. Previously, we have shown that RFT can be applied to control for FWE across 2D time–frequency SPMs, when the sensor-space of interest can be defined a priori [Kilner, Kiebel and Friston (2005)].

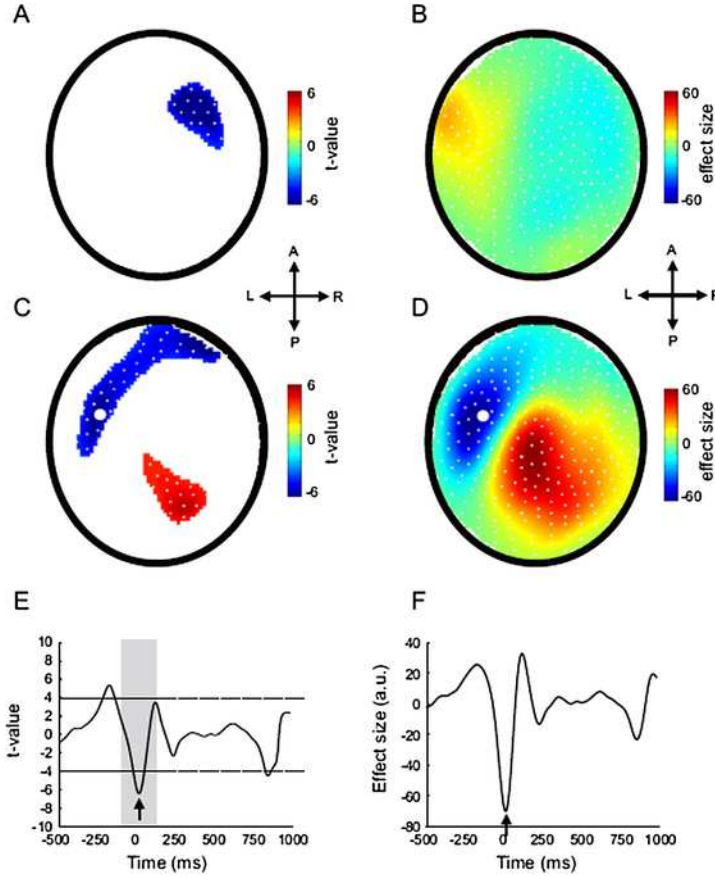


FIG. 2. SPM analysis of movement ERF. (A) shows the SPM( $t$ ), thresholded at  $p < 0.001$  (uncorrected), showing where the effects were less than the mean. The peak value within this cluster is significant at  $p < 0.05$  (FWE corrected). (B) shows the sensor-space map of (nonstandardized) effect size across all sensors at the time where the SPM was maximal. The effect size is proportional to the grand mean across subjects. (C) shows the SPM, thresholded at  $p < 0.001$  (uncorrected), showing where the effects were greater and less than the mean. The sensor within these clusters that was significant at  $p < 0.05$  (corrected for a small search volume) is shown by the white circle. (D) shows the sensor-space map of effect size across all sensors at the time point where the SPM in (C) was maximal. (E) shows the time course of the SPM from the sensor shown in white in (C). The dashed lines show the uncorrected threshold for the Student's  $t$ -statistic at  $p < 0.001$ . (F) shows the corresponding plot for the effect size. In both (E) and (F) the arrow shows the time where the SPM was maximal.

Here, we show that when the frequency band of interest can be specified a priori (often an easier specification), the resulting time-dependent modulation of power in that frequency range can be treated in an identical fashion to the ERF analysis described above. In other words, the 4D data-features

TABLE 1

Statistical results of a full volume analysis in SPM8. The table entries (from left to right) represent the following: the adjusted or corrected  $p$ -value based on random field theory that controls false positive rate; the equivalent  $p$ -value ( $q$ -value) controlling false discovery rate; the maximum Student's  $t$ -statistic; its  $Z$ -score equivalent; its uncorrected  $p$ -value; the time at which this peak occurred. The footnotes provide details of the search volume and topological features expected under the null hypothesis (see <http://www.fil.ion.ucl.ac.uk/spm/> for details)

| Peak level            |                       |      |      |                          |           |
|-----------------------|-----------------------|------|------|--------------------------|-----------|
| $p_{\text{FWE-corr}}$ | $p_{\text{FDR-corr}}$ | $t$  | $Z$  | $p_{\text{uncorrected}}$ | Time (ms) |
| 0.036                 | 0.017                 | 8.71 | 4.80 | 0.000                    | -120      |

Statistics:  $p$ -values restricted to the entire search volume. Height threshold:  $T = 3.93$ ,  $p = 0.001$  (0.993); Degrees of freedom = [1.0, 12.0]; Extent threshold:  $k = 0$  bins,  $p = 1.000$  (0.993); Smoothness FWHM = 13.1 17.5 8.6 {bins}; Expected bins per cluster,  $\langle k \rangle = 121.669$ ; Search vol.: 1,808,083 bins; 230.3 resels; Expected number of clusters,  $\langle c \rangle = 4.96$ ; Expected false discovery rate,  $\leq 0.03$ .

reduce to 3D, by averaging out frequency. In this example, we averaged across frequency bins in the 15–30 Hz range [Figure 3(B)].

The space-time SPM for effects greater than the mean was calculated using a one-sampled  $t$ -test as for the ERF analysis above. A large spatial cluster contained a peak-value that was greater than the threshold corrected for the entire search volume [ $p < 0.05$  corrected: Figure 4(A) and Table 3]. The peak occurred 560 ms after the button press and was within central sensors over both the left and right hemispheres [Figure 4(A)—the sensor at the peak value is indicated by the white circle—and Table 1]. Figure 4(B) shows the average (nonstandardized) effect-size across sensor-space at 560 ms. When comparing the thresholded SPM [Figure 4(A)] and the effect-size map [Figure 4(B)], it is clear that the sensor at the peak of the SPM is

TABLE 2

Statistical results of a small volume analysis in SPM8. This table uses the same format as Table 1

| Peak level            |                       |      |      |                          |           |
|-----------------------|-----------------------|------|------|--------------------------|-----------|
| $p_{\text{FWE-corr}}$ | $p_{\text{FDR-corr}}$ | $t$  | $Z$  | $p_{\text{uncorrected}}$ | Time (ms) |
| 0.013                 | 0.007                 | 6.86 | 4.29 | 0.000                    | 10        |

Statistics:  $p$ -values restricted to -100–100 ms. Height threshold:  $T = 3.93$ ,  $p = 0.001$  (0.289); Degrees of freedom = [1.0, 12.0]; Extent threshold:  $k = 0$  bins,  $p = 1.000$  (0.289); Smoothness FWHM = 13.1 17.5 8.6 {bins}; Expected bins per cluster,  $\langle k \rangle = 121.669$ ; Search vol.: 82,340 bins; 11.5 resels; Expected number of clusters,  $\langle c \rangle = 0.34$ ; Expected false discovery rate,  $\leq 0.01$ .

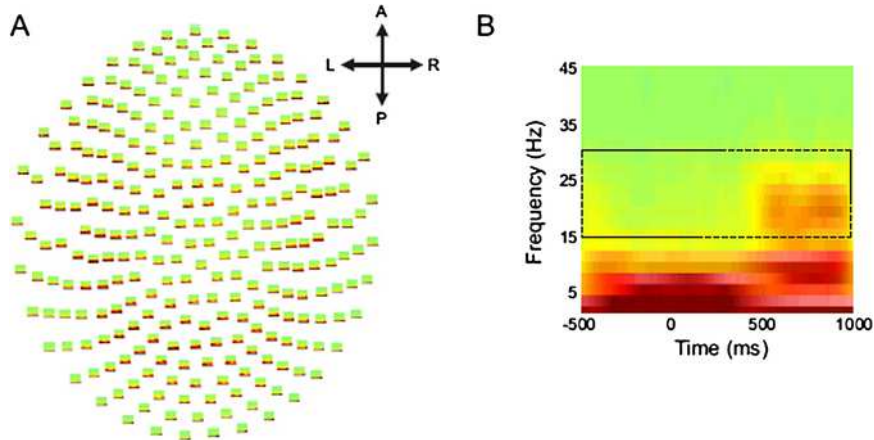


FIG. 3. *Single-subject time–frequency data.* (A) shows the average TF data across trials for the same subject shown in Figure 1. The data are plotted for 275 sensors across peri-stimulus time. (B) shows the average TF data across trials from a single sensor. For the subsequent analysis, the TF maps were averaged across the 15–30 Hz frequency band for each sensor. This band is shown in (B) by the dotted lines.

one of the sensors where the effect is maximal [see also Figures 4(C) and (D)]. Note that in the effect-size map [Figure 4(B)], the dipole field effects observed in Figure 2(D) have the same sign, as the frequency decomposition renders the data-features positive.

**4. Discussion.** We have illustrated how RFT can be employed to control FWE when making statistical inference on continuous data, using movement-related MEG responses that are continuous in space and time. We have not introduced any novel methodology or statistical results. We have simply emphasized the fact that established random field theory can be applied directly to smooth, continuous data-features that conform to its assumptions. The use of RFT may be particularly relevant for EEG and MEG data analysis, which has to deal with data on manifolds that are not simple images and may have a complicated geometry. In one sense, the contribution here is to assert that one does not need novel methods for analyzing EEG and MEG data-features, provided they exhibit continuity or smoothness properties over connected vertices (or voxels). This is because inference is based on topological quantities that do not depend on the coordinates or geometry of those vertices (or voxels).

4.1. *Random field theory assumptions.* One of the assumptions of RFT is that the error fields conform to a good lattice approximation of an underlying random field [Worsley (2007)]. In other words, the underlying random

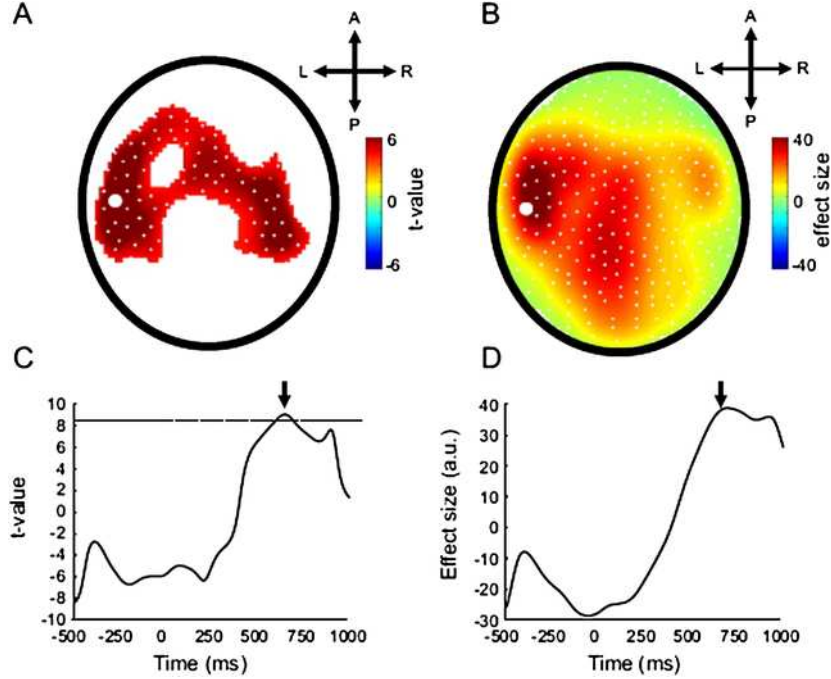


FIG. 4. *SPM analysis of beta rebound. (A) shows the SPM( $t$ ), thresholded at  $p < 0.001$  (uncorrected), showing where the effects were greater than the mean. The peak value within this cluster is significant at  $p < 0.05$  (corrected). The most significant sensor is shown by a white circle. (B) shows the sensor-space map of effect size across all sensors at the time where the SPM was maximal. (C) shows the time course of the SPM from the sensor shown in white in (A). The dashed lines show the FWE corrected threshold for the Student's  $t$ -statistic at  $p < 0.05$ . (D) shows the corresponding plot for the effect size. In both (C) and (D) the arrow shows the time where the SPM was maximal.*

TABLE 3

*Statistical results of the time–frequency analysis in SPM8. See Table 1 for details of the format*

| Peak level            |                       |      |      |                          |           |
|-----------------------|-----------------------|------|------|--------------------------|-----------|
| $p_{\text{FWE-corr}}$ | $p_{\text{FDR-corr}}$ | $t$  | $Z$  | $p_{\text{uncorrected}}$ | Time (ms) |
| 0.033                 | 0.001                 | 9.05 | 4.75 | 0.000                    | 560       |

Statistics:  $p$ -values restricted to the entire search volume. Height threshold:  $T = 4.02$ ,  $p = 0.001$  (0.966); Degrees of freedom = [1.0, 11.0]; Extent threshold:  $k = 0$  bins,  $p = 1.000$  (0.966); Smoothness FWHM = 13.3 13.4 17.1 {bins}; Expected bins per cluster,  $\langle k \rangle = 175.646$ ; Search vol.: 1,808,083 bins; 149.4 resels; Expected number of clusters,  $\langle c \rangle = 3.40$ ; Expected false discovery rate,  $\leq 0.01$ .

field must be sampled sufficiently densely so as to be able to estimate the smoothness of the underlying random field. In practice, this means that one must ensure that there is a sufficiently high sampling of EEG/MEG signals across the dimensions of interest. In the examples presented above these would be sensor-space and time. For high-density EEG and MEG, with a large number of sensors covering the scalp surface, this requirement is clearly met. However, care must be taken if one wanted to adopt this approach for sparsely sampled EEG/MEG data, as this assumption may be violated. In such cases, it is noteworthy that RFT can accommodate any  $D$ -dimensional search-spaces and can therefore be applied to time-courses from a single sensor or some summary over sensors [cf. Carbonell et al. (2004)].

RFT requires that the random fields are multivariate Gaussian with a differentiable correlation function [Worsley (2007)]. The correlations do not have to be stationary when controlling the FWE. This means that any non-stationarity that is induced by flattening a manifold in 3D-space to a 2D sensor-space does not violate the assumptions of RFT. RFT procedures can be used to characterize other topological features of the SPM, namely, the extent and number of clusters. When using RFT to control the FWE rate for cluster-size inference, one effectively measures the size of each cluster in resels, which accommodates local smoothness. It should be noted, however, that the current *SPM8* implementation does not do this properly (for reasons of computational expediency) and that inference on cluster-size assumes isotropic smoothness, which is usually induced by smoothing the data [see also Salmond et al. (2002)]. In the absence of this smoothing, better approximations are available (e.g., *SurfStat*).

Topological inference enables the control of FWE rate across a search volume when making statistical inferences. Therefore, the approach can be adopted in any situation in which one would normally perform parametric statistical tests, such as a  $t$ - or  $F$ -test. When parametric statistical tests cannot be used, for example, when the errors are not normally distributed, the requisite null distribution of the maximal statistic can be estimated using nonparametric procedures. Nonparametric methods have been used to make statistical inference on both MEG source-space data [Singh, Barnes and Hillebrand (2003); Pantazis et al. (2005)] and on clusters in space, time and frequency [Maris and Oostenveld (2007), see also <http://www.ru.nl/neuroimaging/fieldtrip/>]. However, the analytic and closed form expressions provided by RFT are based on assumptions that, if met, render it more powerful or sensitive than equivalent nonparametric approaches [Howell (1997)]. Furthermore, with appropriate transformations [e.g., Kiebel, Tallon-Baudry and Friston (2005)] and post hoc smoothing, it is actually quite difficult to contrive situations where the errors are not multivariate Gaussian (by the central limit theorem) and violate the assumptions of RFT.

4.2. *Topological inference in space and time.* In this note we have shown how RFT can be used to solve the multiple comparisons problem that besets statistical inference using EEG/MEG data. This approach has several advantages. First, it avoids ad hoc or selective characterization of data inherent in conventional approaches that use averages over pre-specified regions of search-space. Second, inference is based on  $p$ -values that are adjusted for multiple nonindependent comparisons, even when dependencies have a complicated form. Third, this adjustment is based explicitly on the search-space, giving the researcher the latitude to restrict the search-space to the extent that prior information dictates. In short, topological inference enables one to test for effects without knowing where they are in space or time. This may be useful, as it could disclose effects that hitherto may have gone untested, for example, small effects that are highly reproducible. However, as we intimated above, the neurophysiological interpretation of significant effects must be considered in light of the quantitative estimates one is making an inference about. In conventional analyses, prior knowledge about the effects of interest is used to average the data to finesse the multiple comparisons problem. With topological inference, these a priori constraints are used to reduce the search-space and adjust the  $p$ -values of the SPM within this reduced volume [Figures 2(C)–(E)]. For example, if one is interested in modulations of the N170, one could reduce the search-space to a time window spanning 140–200 ms post-stimulus. If, in addition, one had predictions about where this effect should be observed in sensor or source space, then one could reduce the search volume even further. The advantage of this, over conventional averaging, is that inference may be more sensitive, as it pertains to peak responses that are necessarily suppressed by averaging.

4.3. *Topological FDR.* We have focused on the use of random field theory for controlling the false positive rate of topological features in statistical maps. However, there is a growing interest in applying the same ideas to control false discovery rate [Benjamini and Hochberg (1995)]. Crucially, topological FDR controls the expected false discovery rate (FDR) of features (such as peaks or excursion sets), as opposed to simply controlling the FDR of point tests (e.g., Student’s  $t$ -tests at each voxel or vertex). This is because FDR procedures in imaging can be problematic and lead to capricious inference [Chumbley and Friston (2009)]. The reason is that most image analysis deals with signals that are continuous (analytic) functions of some support; for example, space or time. In the absence of bounded support, the false discovery rate must be zero. This is because every discovery is a true discovery, given that the signal is (strictly speaking) everywhere. Crucially, one can finesse this problem by inferring on the topological features of the signal. For example, one can assign a  $p$ -value to each local maximum in an SPM using random field theory and identify an adaptive threshold that controls

false discovery rate, using the Benjamini and Hochberg procedure [Chumbley et al. (2010)]. This is called topological FDR and provides a natural complement to conventional FWE control. The notion of topological FDR was introduced in a paper that was the last to be co-authored by Keith Worsley, shortly before his death.

4.4. *Conclusion.* We have illustrated how topological inference can be applied to EEG/MEG data-features that vary as a smooth function of frequency, time or space and have stressed the generality of this application. These procedures have a number of advantages: (i) They require no a priori specification of where effects are expressed, (ii) inferences are based on  $p$ -values that are adjusted for multiple comparisons of continuous and highly correlated data-features and (iii) these inferences are potentially more sensitive than tests on regional averages. One might anticipate that the advances made by Keith Worsley will find new and important domains of application as people start to appreciate the generality and simplicity of his legacy.

**Acknowledgments.** We would like to thank Stefan Kiebel for helpful comments on an earlier version of this manuscript.

## REFERENCES

- BARNES, G. and HILLEBRAND, A. (2003). Statistical flattening of MEG beamformer images. *Human Brain Mapping* **18** 1–12.
- BENJAMINI, Y. and HOCHBERG, Y. (1995). Controlling the false discovery rate—a practical and powerful approach to multiple testing. *J. R. Stat. Soc. Ser. B Stat. Methodol.* **57** 289–300. [MR1325392](#)
- CARBONELL, F., GALÁN, L., VALDÉS, P., WORSLEY, K., BISCAY, R. J., DÍAZ-COMAS, L., BOBES, M. A. and PARRA, M. (2004). Random field-union intersection tests for EEG/MEG imaging. *NeuroImage* **22** 268–276.
- CHEN, C. C., KIEBEL, S. J. and FRISTON, K. J. (2008). Dynamic causal modelling of induced responses. *NeuroImage* **41** 1293–1312.
- CHUMBLEY, J. R. and FRISTON, K. J. (2009). False discovery rate revisited: FDR and topological inference using Gaussian random fields. *NeuroImage* **44** 62–70.
- CHUMBLEY, J., WORSLEY, K., FLANDIN, G. and FRISTON, K. (2010). Topological FDR for neuroimaging. *NeuroImage* **41** 3057–3064.
- FRISTON, K. J., FRITH, C. D., LIDDLE, P. F. and FRACKOWIAK, R. S. J. (1991). Comparing functional (PET) images: The assessment of significant change. *Journal of Cerebral Blood Flow and Metabolism* **11** 690–699.
- FRISTON, K. J., WORSLEY, K. J., FRACKOWIAK, R. S. J., MAZZIOTTA, J. C. and EVANS, A. C. (1994). Assessing the significance of focal activations using their spatial extent. *Human Brain Mapping* **1** 214–220.
- FRISTON, K. J., HOLMES, A. P., WORSLEY, K. J., POLINE, J. B., FRITH, C. D. and FRACKOWIAK, R. S. J. (1995). Statistical parametric maps in functional imaging: A general linear approach. *Human Brain Mapping* **2** 189–210.
- GARRIDO, M. I., FRISTON, K. J., KIEBEL, S. J., STEPHAN, K. E., BALDEWEG, T. and KILNER, J. M. (2008). The functional anatomy of the MMN: A DCM study of the roving paradigm. *NeuroImage* **42** 936–944.

- HARI, R. and IMADA, T. (1999). Ipsilateral movement-evoked fields reconsidered. *NeuroImage* **10** 582–588.
- HARRISON, L. M., PENNY, W., DAUNIZEAU, J. and FRISTON, K. J. (2008). Diffusion-based spatial priors for functional magnetic resonance images. *NeuroImage* **41** 408–423.
- HENSON, R. N., MATTOU, J., SINGH, K. D., BARNES, G. R., HILLEBRAND, A. and FRISTON, K. (2007). Population-level inferences for distributed MEG source localization under multiple constraints: Application to face-evoked fields. *NeuroImage* **38** 422–438.
- HOWELL, D. C. (1997). *Statistical Methods in Psychology*, 4th ed. 121–125. Duxbury Press, Belmont, CA.
- KIEBEL, S. J. and FRISTON, K. J. (2004). Statistical parametric mapping for event-related potentials: I. Generic considerations. *NeuroImage* **22** 492–502.
- KIEBEL, S. J., TALLON-BAUDRY, C. and FRISTON, K. J. (2005). Parametric analysis of oscillatory activity as measured with EEG/MEG. *Human Brain Mapping* **26** 170–177.
- KIEBEL, S. J., POLINE, J. B., FRISTON, K. J., HOLMES, A. P. and WORSLEY, K. J. (1999). Robust smoothness estimation in statistical parametric maps using standardized residuals from the general linear model. *NeuroImage* **10** 756–766.
- KILNER, J. M., KIEBEL, S. J. and FRISTON, K. J. (2005). Applications of random field theory to electrophysiology. *Neurosci. Lett.* **374** 174–175.
- KILNER, J. M., MARCHANT, J. and FRITH, C. D. (2006). Modulation of the mirror system by social relevance. *Social Cognitive and Affective Neuroscience* **1** 143–148.
- KRIEGESKORTE, N., SIMMONS, W. K., BELLGOWAN, P. S. and BAKER, C. I. (2009). Circular analysis in systems neuroscience: The dangers of double dipping. *Nat. Neurosci.* **12** 535–540.
- MARIS, E. and OOSTENVELD, R. (2007). Nonparametric statistical testing of EEG- and MEG-data. *J. Neurosci. Methods* **164** 177–190.
- PANTAZIS, D., NICHOLS, T. E., BAILLET, S. and LEAHY, R. M. (2005). A comparison of random field theory and permutation methods for the statistical analysis of MEG data. *NeuroImage* **25** 383–394.
- PARK, H., KWON, J., YOUN, T., PAE, J., KIM, J., KIM, M. and HA, K. (2002). Statistical parametric mapping of LORETA using high density EEG and individual MRI: Application to mismatch negativities in schizophrenia. *Human Brain Mapping* **17** 168–178.
- RAMSAY, J. O. and SILVERMAN, B. W. (2005). *Functional Data Analysis*, 2nd ed. Springer, New York. [MR2168993](#)
- SALMELIN, R. and HARI, R. (1994). Spatiotemporal characteristics of sensorimotor neuromagnetic rhythms related to thumb movement. *Neuroscience* **60** 537–550.
- SALMOND, C. H., ASHBURNER, J., VARGHA-KHADEM, F., CONNELLY, A., GADIAN, D. G. and FRISTON, K. J. (2002). Distributional assumptions in voxel-based morphometry. *NeuroImage* **17** 1027–1030.
- SINGH, K. D., BARNES, G. R. and HILLEBRAND, A. (2003). Group imaging of task-related changes in cortical synchronisation using nonparametric permutation testing. *NeuroImage* **19** 1589–1601.
- TAYLOR, J. E. and WORSLEY, K. J. (2007). Detecting sparse signal in random fields, with an application to brain mapping. *J. Amer. Statist. Assoc.* **102** 913–928. [MR2354405](#)
- WORSLEY, K. J. (2007). Random field theory. In *Statistical Parametric Mapping*, Chapter 18. Academic Press, London, UK.
- WORSLEY, K. J., EVANS, A. C., MARRETT, S. and NEELIN, P. (1992). A three dimensional statistical analysis for CBF activation studies in the human brain. *Journal of Cerebral Blood Flow and Metabolism* **12** 900–918.

- WORSLEY, K. J., MARRETT, S., NEELIN, P., NANDAL, A. C., FRISTON, K. J. and EVANS, A. C. (1996). A unified statistical approach for determining significant voxels in images of cerebral activation. *Human Brain Mapping* **4** 58–73.
- WORSLEY, K. J., ANDERMANN, M., KOULIS, T., MACDONALD, D. and EVANS, A. C. (1999). Detecting changes in non-isotropic images. *Human Brain Mapping* **8** 98–101.
- WORSLEY, K. J., LIAO, C., ASTON, J., PETRE, V., DUNCAN, G. H., MORALES, F. and EVANS, A. C. (2002). A general statistical analysis for fMRI data. *NeuroImage* **15** 1–15.

INSTITUTE OF NEUROLOGY  
UNIVERSITY COLLEGE LONDON  
THE WELLCOME TRUST CENTRE FOR NEUROIMAGING  
12 QUEEN SQUARE  
LONDON WC1N 3BG  
UNITED KINGDOM  
E-MAIL: [k.friston@fil.ion.ucl.ac.uk](mailto:k.friston@fil.ion.ucl.ac.uk)